4-18-2014

Lifshitz Transition and Chemical Instabilities in Ba1−xKxFe2As2 Superconductors

Suffian N. Khan
Ames Laboratory

Duane D. Johnson
Iowa State University, ddj@iastate.edu

Lifshitz Transition and Chemical Instabilities in Ba1−xKxFe2As2 Superconductors

Abstract
For solid-solution Ba1−xKxFe2As2 Fermi surface evolution is mapped via Bloch spectral functions calculated using density functional theory implemented in Korringa-Kohn-Rostoker multiple scattering theory with the coherent-potential approximation. Spectral functions reveal electronic dispersion, topology, orbital character, and broadening (electron-lifetime effects) due to chemical disorder. Dissolution of electron cylinders occurs near x~0.9 with a nonuniform, topological (Lifshitz) transition, reducing the interband interactions; yet the dispersion maintains its dxz or dyz character. Formation energies indicate alloying at x=0.35, as observed, and a tendency for segregation on the K-rich (x>0.6) side, explaining the difficulty of controlling sample quality and the conflicting results between characterized electronic structures. Our results reveal Fermi surface transitions in alloyed samples that influence s± to nodal superconductivity and suggest the origin for deviations of common trends in Fe-based superconductors, such as Bud'ko-Ni-Canfield scaling.

Keywords
Materials Science and Engineering

Disciplines
Condensed Matter Physics | Engineering Physics | Materials Science and Engineering

Comments
This article is from Phys. Rev. Lett. **112**, 156401 (2014), doi:10.1103/PhysRevLett.112.156401. Posted with permission.

Lifshitz Transition and Chemical Instabilities in $Ba_{1-x}K_xFe_2As_2$ Superconductors

Suffian N. Khan[1,2,*] and Duane D. Johnson[1,2,3,†]
[1]Department of Physics, University of Illinois, Urbana-Champaign, Illinois 61801, USA
[2]The Ames Laboratory, U.S. Department of Energy, Ames, Iowa 50011-3020, USA
[3]Department of Materials Science & Engineering, Iowa State University, Ames, Iowa 50011-2300, USA
(Received 11 November 2013; published 14 April 2014)

For solid-solution $Ba_{1-x}K_xFe_2As_2$ Fermi surface evolution is mapped via Bloch spectral functions calculated using density functional theory implemented in Korringa-Kohn-Rostoker multiple scattering theory with the coherent-potential approximation. Spectral functions reveal electronic dispersion, topology, orbital character, and broadening (electron-lifetime effects) due to chemical disorder. Dissolution of electron cylinders occurs near $x \sim 0.9$ with a nonuniform, topological (Lifshitz) transition, reducing the interband interactions; yet the dispersion maintains its d_{xz} or d_{yz} character. Formation energies indicate alloying at $x = 0.35$, as observed, and a tendency for segregation on the K-rich ($x > 0.6$) side, explaining the difficulty of controlling sample quality and the conflicting results between characterized electronic structures. Our results reveal Fermi surface transitions in alloyed samples that influence $s^{\pm}$ to nodal superconductivity and suggest the origin for deviations of common trends in Fe-based superconductors, such as Bud'ko-Ni-Canfield scaling.

DOI: 10.1103/PhysRevLett.112.156401 PACS numbers: 71.18.+y, 74.20.Pq, 74.70.Xa

Superconductivity in Fe-based superconductors (Fe SCs) is achieved by chemical substitution or applied pressure to tune geometry and charge [1–6]. Lifshitz transitions can mark the onset of SC [7,8,17]. Among Fe SCs, $Ba_{1-x}K_xFe_2As_2$ (BKFA) stands out for featuring a number of anomalies in the heavily overdoped (HOD) regime, including an apparent Fermi-surface transition, and violation of "universal" trends found in most Fe SCs. Making homogenous samples of HOD BKFA has proven difficult, which has not been explained. Reliable comparison of electronic properties between various experiments has also been an issue.

For nonmagnetic, tetragonal ($I4/mmm$) BKFA, we use density functional theory (DFT) to detail the Fermi-surface topology and character, and locate dissolution of electron pockets and onset of hole blades. The Fermi surface is mapped from overdoped $x \geq 0.6$, and exhibits a Lifshitz transition near $x = 0.9$. In Fe SCs, the $s^{\pm}$ gap symmetry is considered closely tied to intraband transitions among hole and electron surfaces [18,41]. The loss of these transitions in HOD BKFA could result in a weakening of spin-fluctuation-mediated pairing and signal competition with orbital fluctuations. Formation energies are calculated for all x, which show chemical instabilities at both underdoping and heavy overdoping. The instabilities highlight the difficulty in preparing uniform samples, explaining the discrepancies between various observed electronic structures. We verify that paramagnetism given by the "disordered local moment" (DLM) state exhibits similar behavior, with no change in conclusions.

Background.—Common Fe SCs features or trends have been identified. The electronic structure is a hybridization of Fe $3d$ and As $4p$ orbitals, which is sensitive to lattice parameters and internal (Fe-As) coordinates. At the experimental lattice parameters, the DFT Fermi surface of the paramagnetic state often exhibits two or three hole cylinders at the zone center (Γ point) and two electron cylinders at the zone corner (X point), which agree well with angle-resolved photoemission (ARPES), e.g., for LiFeAs (LFA), $BaFe_2As_2$ (BFA), and LaFeAsO (LFAO) [9–12]. This electronic structure plays a key role in defining the magnetic and SC ground states. In BFA and LFAO there is prominent (π, π) nesting between hole and electron cylinders, in correspondence with the observed antiferromagnetic (AFM) ordering [13,14]. Moreover, when nesting becomes imperfect, as in $Ba(Fe_{1-x}Co_x)_2As_2$ (BFCA), the magnetic ordering becomes incommensurate spin-density wave [15]; in LFA, where nesting is absent, the ground state is nonmagnetic [11]. Also, spin fluctuations (SF) in this mode have been correlated to SC [16,17]. Taking this SF as the dominant pairing mechanism requires an $s^{\pm}$ gap symmetry, i.e., cylindrical nodes [18], as also evidenced from a resonance in spin susceptibility [19–21]. Further universality includes a common trend between the As-Fe-As bond angle and the critical temperature T_c [22], and the linear BNC scaling [23], i.e., specific heat jump $\Delta c_S \propto T_c^3$.

In KFe_2As_2 (KFA) there are well-defined vertical line nodes on one of the hole cylinders and a total dissolution of electron pockets [24], and hole blades appear about X [25]. Application of pressure shows critical behavior in the T_c response [26]. Universal heat conduction is suggestive of a d-wave symmetry and possibly a neighboring quantum critical point [27–30]. The K concentration (x) at which this transition occurs and what characterizes the transition is still under debate. In one study BKFA fails to follow the BNC scaling at $x = 0.7$–0.8 [31]. An ARPES study sees an abrupt change in the gap magnitude occurring near $x = 0.6$,

TABLE I. For each sphere, Wyckoff ($I4/mmm$) positions and coordinates in face-centered cell with Ba at the corners.

$E1$	$2b$	$(0.5000a, 0.0000a, 0.0000c)$
$E2$	$4e$	$(0.0000a, 0.0000a, 0.2072c)$
$E3$	$16m$	$(0.2007a, 0.0000a, 0.1715c)$

simultaneously with a Lifshitz transition [32]. Still other studies continue to see electron pockets without hole blades at $x = 0.7$ and estimate a transition at $x = 0.8$–0.9 [33]. Andreev reflection finds no transition up to $x = 0.77$ [34]. And, some studies see hole blades as early as optimal doping ($x = 0.4$) [35], and others do not [36]. Complicating measurements is the instability of homogenous samples at HOD and low T_c [37].

The BKFA phase diagram ($0 \leq x \leq 1$) is known [38,39]. BFA is a compensated metal in a low-temperature $Fmmm$ structure with striped AFM [13]. KFA is a nonmagnetic SC in $I4/mmm$ structure exhibiting only hole carriers [25]. Optimal doping is achieved at $x = 0.4$ with $T_c = 38$ K. A coexistence between AFM and SC exists for $0.1 < x < 0.25$, though evidence suggests this is due to inhomogeneity in the sample [38]. Optimal doping has the hallmarks of an Fe SC, including nested hole and electron cylinders and $s^{\pm}$ gap symmetry [36,40]. Nested surfaces have the same energy gap, suggesting active transitions between these states [41]. Steric effects, e.g., the As-Fe-As bond angle, can account for optimal doping at $x = 0.4$, where $FeAs_4$ form ideal tetrahedra, and also for diminishing T_c with $x > 0.4$ [38]. However, it does not explain the transition to nodal SC and other HOD anomalies.

Calculation details.—DFT calculations were performed using an all-electron, Korringa-Kohn-Rostoker (KKR) Green's function method within the coherent potential approximation (CPA) [42–44]. The methods applied here have explained the spin-density wave behavior and scattering data in $Ba(Fe_{1-x}M_x)_2As_2$ versus solute (M = Co, Ni, Cu) [15], and the quantum criticality in $NbFe_2$ from an alloying-mediated Lifshitz transition at an unconventional band critical point [45]. To improve the basis set, empty spheres ($E1$, $E2$, and $E3$) were inserted in the structure (Table I). Sphere sizes were maximized in the order Ba, Fe(= As), $E1$, $E2$, and $E3$. The same sphere positions were used for the orthorhombic ($Fmmm$) structures. All results were obtained with a $16 \times 16 \times 16$ Monkhort-Pack k-point mesh for Brillouin zone (BZ) integrals [46], and using complex energy (E) contour integration with 25 E points on a Gauss-Legendre semicircular contour [47]. The valence configurations were taken as Ba $5p^6 6s^2$, K $3p^6 4s^1$, Fe $4s^2 3d^6$, and As $4s^2 4p^3$. Fermi energies were determined via the analytic Lloyd's formula for an accurate electron count [48]. To avoid DFT sensitivity to structure, we used measured structural parameters versus x for both $Fmmm$ and $I4/mmm$ structures [39]. However, for $I4/mmm$, the experimental data are limited versus x, but show that Vegard's law [49] is invalid. But, two linear regimes match experiment well (1) from $x = 0$–0.3, and (2) from $x = 0.3$–1.0.

Fermi surfaces are determined via the Bloch spectral function $A(\mathbf{k}, E) = -(1/\pi)\mathrm{Im}G(\mathbf{k}, \mathbf{k}, E)$, where G is the single-particle Green's function. $A(\mathbf{k}, E)$ is the E and $\mathbf{k}$-space resolved density of states and dispersion. In the limit of an ordered compound it reduces to Dirac δ functions that define the band structure $E(\mathbf{k})$. For $x \neq 0$ or 1 there is $\mathbf{k}$-dependent spectral broadening and shifting due to chemical disorder (impurity scattering) handled via the CPA. The spectral full width at half maximum with respect to energy is inversely proportional to the lifetime of electronic states.

Results.—For $Ba_{1-x}K_xFe_2As_2$ ($x \geq 0.6$), we find a Lifshitz transition in the Fermi surface evolution (Fig. 1), as is clearly evident at the X point near $x = 0.9$. Spectral intensity is scaled according to a false color map given in Fig. 2(a). The BZ with high-symmetry labels is provided in Fig. 2(a). Cross sections in Fig. 1 are along the $k_x - k_z$ (top) and $k_x - k_y$ (bottom) plane. A corresponding cut in both planes is shown as a dashed line at $x = 0.85$. A 4_1-screw symmetry along k_z is obeyed at the X point.

As BKFA approaches KFA (i.e., $x \to 1$), holes centered at Γ grow and electrons at X shrink. Near the critical concentration $x_c = 0.9$ the electrons disappear and hole blades appear. We find from $x = 0.6$ to 0.85 the electron pockets have shrunk without topological change. Just before the transition the bands flatten. Each electron pocket

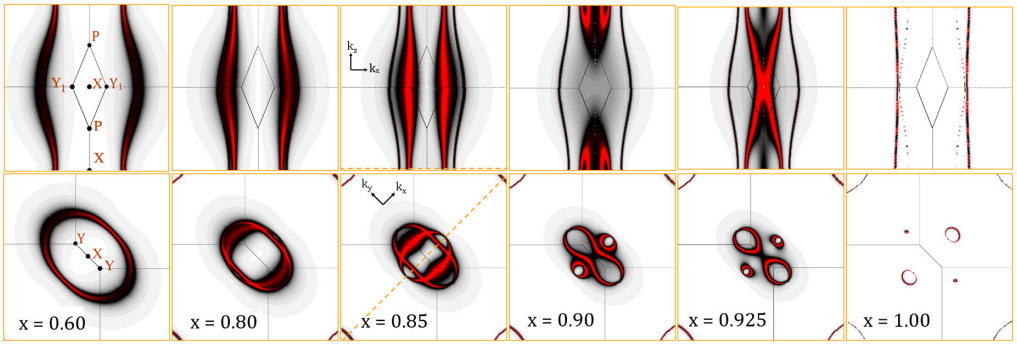

FIG. 1 (color online). $Ba_{1-x}K_xFe_2As_2$ Fermi surface evolution of electron cylinders versus K content. Intensity is in units of 10^3 states $\mathrm{Ryd}^{-1}\mathrm{cell}^{-1}$, with scale bar in Fig. 2. Top (bottom): Bloch spectral function along (010) [(001)] planes in k space. Solid lines indicate BZ boundaries. Thick dashed lines indicate corresponding cuts between the top and bottom panels.

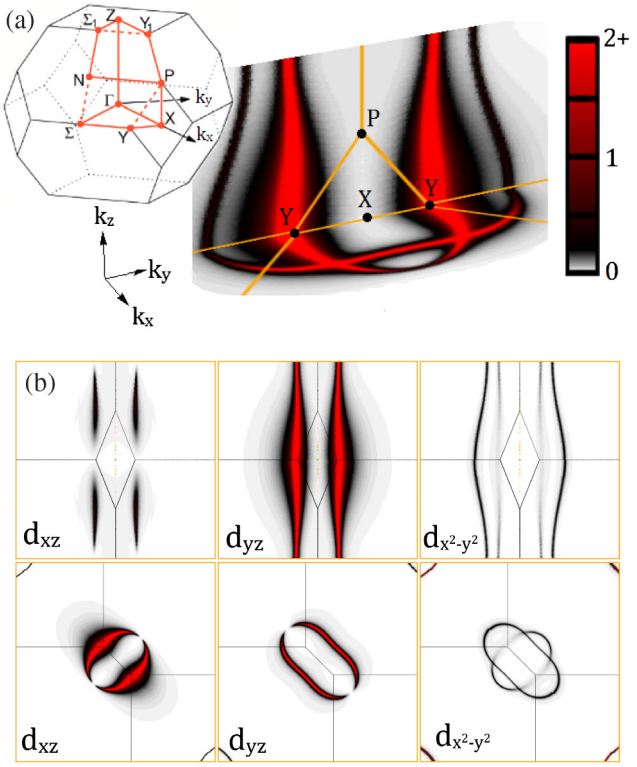

FIG. 2 (color online). (a) Fermi surfaces near X points (3D perspective) for nonmagnetic, tetragonal $Ba_{0.15}K_{0.85}Fe_2As_2$ in units of 10^3 states $Ryd^{-1}cell^{-1}$. Cylinderlike electron sheets are evident. Inset shows BZ with symmetry labels (the BZ height shrinks as x increases). (b) Electron cylinders are decomposed into Fe-site orbital projections. x and y directions in real space coincide with neighboring Fe-Fe bonds in the Fe square net. Spectral intensities projected by character do not follow the symmetry of the crystal.

maintains its own character (cf. Fig. 2) and undergoes transitions separately. The electron cylinder with a major axis along k_x splits first between $0.85 < x < 0.90$. Three dimensionality at $x = 0.9$ is apparent in the top frame. Hole pockets then appear lateral to X. The second electron cylinder with a major axis along k_y undergoes a split between $0.90 < x < 0.925$. Subsequently, two additional hole cylinders are established just before $x = 1$, and at the end point all Fermi surfaces are holelike. The density of states $n(E)$ is not peaked at the Lifshitz point, suggesting a more involved relation to SC.

For further perspective, at $x = 0.85$, just before the Lifshitz transition, we plot the orbital decomposition [Fig. 2(b)] and the dispersion (Fig. 3). The evolution of the transition can be more reliably ascertained at this concentration (rather than the end compounds) by shifting the Fermi energy (E_F) in Fig. 3 up across the Lifshitz transition (e^- doping) or down (h^+ doping). The "band" broadening is ~50 meV in energy, comparable to the band shifts needed to match DFT and ARPES [2]. The k-space broadening is ~0.03 reciprocal lattice units. The electron and hole pockets are osculating; the dissolution of electrons and appearance of holes is nearly simultaneous. Traveling from Γ to X across E_F, the first three band crossings

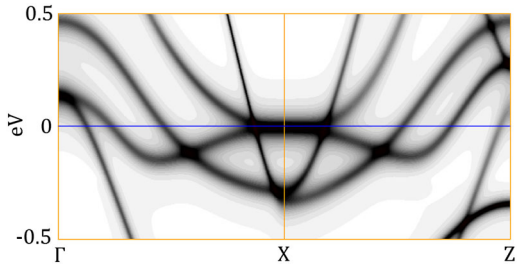

FIG. 3 (color online). Electronic dispersion (Bloch spectral functions) of $Ba_{0.15}K_{0.85}Fe_2As_2$ near Fermi energy (0 eV) from Γ = [000] to X = [100] to Z = [110]. Spectral broadening is evident.

correspond to hole cylinders about Γ. The next two crossings represent either the outer and inner e^- pockets about X (above E_F), or a single hole cylinder (below E_F). Similar crossings occur traveling from Z to X. The bands that cross E_F arise from Fe $3d$ orbitals. The character of electron pockets [Fig. 2(b)] is majority d_{xz} and d_{yz} character, with some $d_{x^2-y^2}$ hybridization. There is a modest d_{z^2} hybridization on the middle band of the hole pocket about Γ (not shown), which compares favorably to line nodes on this hole cylinder found in ARPES [24]. However, the experiment places the d_{z^2} band closer to E_F, and crossing at KFA. The $d_{x^2-y^2}$ correspond to the direct Fe-Fe σ bond.

Finally, formation energies (ΔE_f) for $Ba_{1-x}K_xFe_2As_2$ solid solutions at 0 K are shown in Fig. 4. A negative ΔE_f indicates that the sample is more favorable than segregating to the end point compounds; however, only those alloys below Maxwell tie lines are globally stable at 0 K, e.g., $x = 0.35$, which is close to optimal doping and where $FeAs_4$ form ideal tetrahedra. This stability is likely enhanced by spectral peak overlap of the two electron cylinders about X near $x = 0.4$ (Fig. S2 [50]). At small x, we find, as observed, the orthorhombic phase is more stable than the tetragonal phase. Tetragonal solid solutions whose ΔE_f lies above the Maxwell tie line are unstable at 0 K to a mixed compound formed from concentrations at the end points of the line segment on the tie line. The Maxwell tie line consists of two segments: one from $x = 0$ to 0.35 and another from $x = 0.35$ to 1.0. This unusual curve reflects in part the variation of the lattice constants versus x, whose slopes change near $x = 0.3$; see Fig. S4 in the Supplemental Material [50]. For underdoping (0.15–0.3) the high-T, tetragonal phase form is slightly unstable to segregation, in agreement with experiment [31]. At nonzero temperatures entropy will favor the disordered states. To account for this, the free energy [51] at the experimental annealing temperature of 1000 K is also shown in Fig. 4, which exhibits similar behavior to ΔE_f (0 K). While the most stable (global) configuration for $x \geq 0.35$ should be an admixture of $Ba_{0.65}K_{0.35}Fe_2As_2$ plus KFe_2As_2, the free energy difference to drive this diffusion-limited state is weak, which explains the large range of concentrations in samples and conflicting reports on properties. For $x > 0.6$, there is a stronger segregation instability, with a maximum near $x = 0.8$ (Fig. 4, inset). Experiments indicate a possible

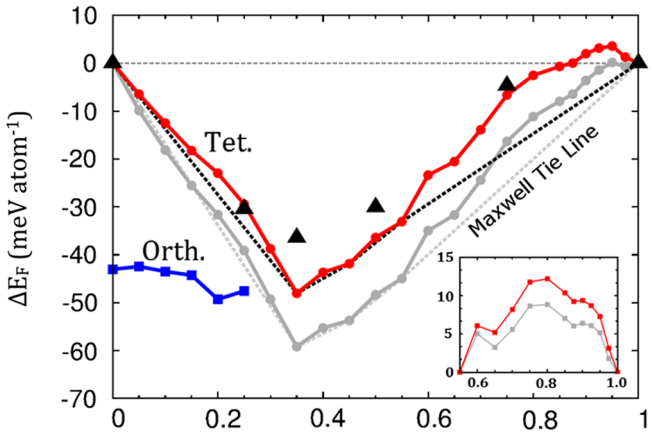

FIG. 4 (color online). ΔE_f (0 K) versus x (red symbols or lines) for $Ba_{1-x}K_xFe_2As_2$, relative to endpoint alloys. The Maxwell tie (dashed) lines are indicated. At 1000 K, the free energy (gray line), using ideal mixing entropy [51], follows the 0 K behavior. At the Ba-rich side, orthorhombic $Ba_{1-x}K_xFe_2As_2$ (blue symbols or lines) is favored, as observed. The DLM states (triangles) show similar behavior to the nonmagnetic cases. Inset shows ΔE_f relative to the tie line between $x = 0.55$ and 1, exhibiting local instability to segregation with maximum at $x \sim 0.8$ for 0–1000 K.

miscibility gap from $x = 0.64$ to 0.82 at a growth temperature of 1000 °C[52].

For completeness, in Fig. 4 we include calculations of ΔE_f (0 K) versus x for the paramagnetic DLM state in which Fe moments of $1.0\mu_B$ are randomly oriented, from a self-consistent electronic structure with spin disorder. These results show very similar energetics to the nonmagnetic ones, indicating both paramagnetic states lead to similar results. Either way, our formation energy results certainly clarify some of the difficulty of controlling sample composition and quality, which is reflected in the associated conflicting results on experimentally characterizing the electronic structure of BKFA.

In summary, among Fe SCs, BKFA is of particular interest because it undergoes a transition at heavy overdoping that has yet to be fully understood, and deviates from known FeSC trends. Making homogenous samples in this concentration range has proved difficult, as explained via our results on stability. Using KKR-CPA methods, we have gone beyond the rigid-band approximation to explore the full concentration range. We find a Lifshitz transition near $x = 0.9$ that occurs in parts; both electron cylinders disappear at slightly different x. The Lifshitz transition marks a reduction of interband transitions and likely a weakening of SF-mediated pairs. The orbital character of the dispersion near the transition is strongly pronounced, unlike that observed on the underdoped side [9]. This may suggest increased competition of spin and orbital fluctuations; there have been SFs observed in KFA at the (π, π) mode [53]. We also find the electronic disorder broadening is comparable to band shifts required for DFT to ARPES to match. The Lifshitz transition behavior detailed here also suggests an explanation for the observed deviation from the linear BNC scaling [23].

More ARPES studies in this regime, and indirect bulk measurements of the Lifshitz transition, such as the Hall coefficient, would connect directly to our results. A reversion from nodal SC to standard $s^{\pm}$ may occur under the application of pressure to KFA [26]. This may also be due to a Lifshitz transition, as electron doping has been found to correlate with pressure for Fe SCs [54]. Studying the Fermi surface response to pressure to see if a Lifshitz response can be ruled out may resolve this. However, the response of T_c with e^- doping is continuous, while response under pressure is discontinuous, suggesting these changes have different origins.

We acknowledge discussions with Paul Canfield, Sergey Bud'ko, and Adam Kaminski. Work was supported by the U.S. Department of Energy, Office of Science, Basic Energy Sciences, Materials Science and Engineering Division at Ames, and through the Center for Defect Physics, an Energy Frontier Research Center at ORNL, for improved techniques to address accurately defects in materials. The Ames Laboratory is operated for the U.S. DOE by Iowa State University under Contract No. DE-AC02-07CH11358.

*snkhan@illinois.edu
†ddj@ameslab.gov

[1] G. R. Stewart, Rev. Mod. Phys. **83**, 1589 (2011).
[2] A. A. Kordyuk, Low Temp. Phys. **38**, 888 (2012).
[3] P. M. Aswathy, J. B. Anooja, P. M. Sarun, and U. Syamaprasad, Supercond. Sci. Technol. **23**, 073001 (2010).
[4] J. Paglione and R. L. Greene, Nat. Phys. **6**, 645 (2010).
[5] H.-H. Wen and S. Li, Annu. Rev. Condens. Matter Phys. **2**, 121 (2011).
[6] P. C. Canfield and S. L. Bud'ko, Annu. Rev. Condens. Matter Phys. **1**, 27 (2010).
[7] C. Liu, T. Kondo, R. M. Fernandes, A. D. Palczewski, E. D. Mun, N. Ni, A. N. Thaler, A. Bostwick, E. Rotenberg, J. Schmalian, S. L. Bud'ko, P. C. Canfield, and A. Kaminski, Nat. Phys. **6**, 419 (2010).
[8] C. Liu, A. D. Palczewski, R. S. Dhaka, T. Kondo, R. M. Fernandes, E. D. Mun, H. Hodovanets, A. N. Thaler, J. Schmalian, S. L. Bud'ko, P. C. Canfield, and A. Kaminski, Phys. Rev. B **84**, 020509 (2011).
[9] M. Yi, D. H. Lu, J. G. Analytis, J.-H. Chu, S.-K. Mo, R.-H. He, R. G. Moore, X. J. Zhou, G. F. Chen, J. L. Luo, N. L. Wang, Z. Hussain, D. J. Singh, I. R. Fisher, and Z.-X. Shen, Phys. Rev. B **80**, 024515 (2009).
[10] D. J. Singh, Phys. Rev. B **78**, 094511 (2008).
[11] S. V. Borisenko, V. B. Zabolotnyy, D. V. Evtushinsky, T. K. Kim, I. V. Morozov, A. N. Yaresko, A. A. Kordyuk, G. Behr, A. Vasiliev, R. Follath, and B. Büchner, Phys. Rev. Lett. **105**, 067002 (2010).
[12] C. Liu, Y. Lee, A. D. Palczewski, J.-Q. Yan, T. Kondo, B. N. Harmon, R. W. McCallum, T. A. Lograsso, and A. Kaminski, Phys. Rev. B **82**, 075135 (2010).
[13] M. Rotter, M. Tegel, D. Johrendt, I. Schellenberg, W. Hermes, and R. Pöttgen, Phys. Rev. B **78**, 020503 (2008).
[14] C. de la Cruz, Q. Huang, J. W. Lynn, J. Li, W. Ratcliff II, J. L. Zarestky, H. A. Mook, G. F. Chen, J. L. Luo, N. L. Wang, and P. Dai, Nature (London) **453**, 899 (2008).

[15] M. G. Kim, J. Lamsal, T. W. Heitmann, G. S. Tucker, D. K. Pratt, S. N. Khan, Y. B. Lee, A. Alam, A. Thaler, N. Ni, S. Ran, S. L. Bud'ko, K. J. Marty, M. D. Lumsden, P. C. Canfield, B. N. Harmon, D. D. Johnson, A. Kreyssig, R. J. McQueeney, and A. I. Goldman, Phys. Rev. Lett. **109**, 167003 (2012).

[16] F. L. Ning, K. Ahilan, T. Imai, A. S. Sefat, M. A. McGuire, B. C. Sales, D. Mandrus, P. Cheng, B. Shen, and H.-H. Wen, Phys. Rev. Lett. **104**, 037001 (2010).

[17] K. Matan, S. Ibuka, R. Morinaga, S. Chi, J. W. Lynn, A. D. Christianson, M. D. Lumsden, and T. J. Sato, Phys. Rev. B **82**, 054515 (2010).

[18] I. I. Mazin, D. J. Singh, M. D. Johannes, and M. H. Du, Phys. Rev. Lett. **101**, 057003 (2008).

[19] A. D. Christianson, E. A. Goremychkin, R. Osborn, S. Rosenkranz, M. D. Lumsden, C. D. Malliakas, I. S. Todorov, H. Claus, D. Y. Chung, M. G. Kanatzidis, R. I. Bewley, and T. Guidi, Nature (London) **456**, 930 (2008).

[20] M. D. Lumsden, A. D. Christianson, D. Parshall, M. B. Stone, S. E. Nagler, G. J. MacDougall, H. A. Mook, K. Lokshin, T. Egami, D. L. Abernathy, E. A. Goremychkin, R. Osborn, M. A. McGuire, A. S. Sefat, R. Jin, B. C. Sales, and D. Mandrus, Phys. Rev. Lett. **102**, 107005 (2009).

[21] S. Chi, A. Schneidewind, J. Zhao, L. W. Harriger, L. Li, Y. Luo, G. Cao, Z. Xu, M. Loewenhaupt, J. Hu, and P. Dai, Phys. Rev. Lett. **102**, 107006 (2009).

[22] C.-H. Lee, A. Iyo, H. Eisaki, H. Kito, M. T. Fernandez-Diaz, T. Ito, K. Kihou, H. Matsuhata, M. Braden, and K. Yamada, J. Phys. Soc. Jpn. **77**, 083704 (2008).

[23] S. L. Bud'ko, N. Ni, and P. C. Canfield, Phys. Rev. B **79**, 220516 (2009).

[24] K. Okazaki, Y. Ota, Y. Kotani, W. Malaeb, Y. Ishida, T. Shimojima, T. Kiss, S. Watanabe, C.-T. Chen, K. Kihou, C. H. Lee, A. Iyo, H. Eisaki, T. Saito, H. Fukazawa, Y. Kohori, K. Hashimoto, T. Shibauchi, Y. Matsuda, H. Ikeda, H. Miyahara, R. Arita, A. Chainani, and S. Shin, Science **337**, 1314 (2012).

[25] T. Yoshida, I. Nishi, A. Fujimori, M. Yi, R. Moore, D.-H. Lu, Z.-X. Shen, K. Kihou, P. Shirage, H. Kito, C. Lee, A. Iyo, H. Eisaki, and H. Harima, J. Phys. Chem. Solids **72**, 465 (2011).

[26] F. F. Tafti, A. Juneau-Fecteau, M.-E. Delage, S. Rene de Cotret, J.-P. Reid, A. F. Wang, X.-G. Luo, X. H. Chen, N. Doiron-Leyraud, and L. Taillefer, Nat. Phys. **9**, 349 (2013).

[27] J.-P. Reid, M. A. Tanatar, A. Juneau-Fecteau, R. T. Gordon, S. R. de Cotret, N. Doiron-Leyraud, T. Saito, H. Fukazawa, Y. Kohori, K. Kihou, C. H. Lee, A. Iyo, H. Eisaki, R. Prozorov, and L. Taillefer, Phys. Rev. Lett. **109**, 087001 (2012).

[28] A. F. Wang, S. Y. Zhou, X. G. Luo, X. C. Hong, Y. J. Yan, J. J. Ying, P. Cheng, G. J. Ye, Z. J. Xiang, S. Y. Li, and X. H. Chen, Phys. Rev. B **89**, 064510 (2014).

[29] W. Li, J. Li, J.-X. Zhu, Y. Chen, and C. S. Ting, Europhys. Lett. **99**, 57 006 (2012).

[30] J. K. Dong, S. Y. Zhou, T. Y. Guan, H. Zhang, Y. F. Dai, X. Qiu, X. F. Wang, Y. He, X. H. Chen, and S. Y. Li, Phys. Rev. Lett. **104**, 087005 (2010).

[31] S. L. Bud'ko, M. Sturza, D. Y. Chung, M. G. Kanatzidis, and P. C. Canfield, Phys. Rev. B **87**, 100509 (2013).

[32] W. Malaeb, T. Shimojima, Y. Ishida, K. Okazaki, Y. Ota, K. Ohgushi, K. Kihou, T. Saito, C. H. Lee, S. Ishida, M. Nakajima, S. Uchida, H. Fukazawa, Y. Kohori, A. Iyo, H. Eisaki, C.-T. Chen, S. Watanabe, H. Ikeda, and S. Shin, Phys. Rev. B **86**, 165117 (2012).

[33] K. Nakayama, T. Sato, P. Richard, Y.-M. Xu, T. Kawahara, K. Umezawa, T. Qian, M. Neupane, G. F. Chen, H. Ding, and T. Takahashi, Phys. Rev. B **83**, 020501 (2011).

[34] X. Zhang, Y. S. Oh, Y. Liu, L. Yan, S. R. Saha, N. P. Butch, K. Kirshenbaum, K. H. Kim, J. Paglione, R. L. Greene, and I. Takeuchi, Phys. Rev. B **82**, 020515 (2010).

[35] D. V. Evtushinsky, D. S. Inosov, V. B. Zabolotnyy, A. Koitzsch, M. Knupfer, B. Büchner, M. S. Viazovska, G. L. Sun, V. Hinkov, A. V. Boris, C. T. Lin, B. Keimer, A. Varykhalov, A. A. Kordyuk, and S. V. Borisenko, Phys. Rev. B **79**, 054517 (2009).

[36] T. Sato, K. Nakayama, Y. Sekiba, P. Richard, Y.-M. Xu, S. Souma, T. Takahashi, G. F. Chen, J. L. Luo, N. L. Wang, and H. Ding, Phys. Rev. Lett. **103**, 047002 (2009).

[37] J. T. Park, D. S. Inosov, C. Niedermayer, G. L. Sun, D. Haug, N. B. Christensen, R. Dinnebier, A. V. Boris, A. J. Drew, L. Schulz, T. Shapoval, U. Wolff, V. Neu, X. Yang, C. T. Lin, B. Keimer, and V. Hinkov, Phys. Rev. Lett. **102**, 117006 (2009).

[38] M. Rotter, M. Pangerl, M. Tegel, and D. Johrendt, Angew. Chem., Int. Ed. Engl. **47**, 7949 (2008).

[39] S. Avci, O. Chmaissem, D. Y. Chung, S. Rosenkranz, E. A. Goremychkin, J. P. Castellan, I. S. Todorov, J. A. Schlueter, H. Claus, A. Daoud-Aladine, D. D. Khalyavin, M. G. Kanatzidis, and R. Osborn, Phys. Rev. B **85**, 184507 (2012).

[40] C. Liu, G. D. Samolyuk, Y. Lee, N. Ni, T. Kondo, A. F. Santander-Syro, S. L. Bud'ko, J. L. McChesney, E. Rotenberg, T. Valla, A. V. Fedorov, P. C. Canfield, B. N. Harmon, and A. Kaminski, Phys. Rev. Lett. **101**, 177005 (2008).

[41] H. Ding, P. Richard, K. Nakayama, K. Sugawara, T. Arakane, Y. Sekiba, A. Takayama, S. Souma, T. Sato, T. Takahashi, Z. Wang, X. Dai, Z. Fang, G. F. Chen, J. L. Luo, and N. L. Wang, Europhys. Lett. **83**, 47001 (2008).

[42] J. Korringa, Physica (Amsterdam) **13**, 392 (1947).

[43] W. Kohn and N. Rostoker, Phys. Rev. **94**, 1111 (1954).

[44] D. D. Johnson, D. M. Nicholson, F. J. Pinski, B. L. Gyorffy, and G. M. Stocks, Phys. Rev. Lett. **56**, 2088 (1986).

[45] A. Alam and D. D. Johnson, Phys. Rev. Lett. **107**, 206401 (2011).

[46] H. J. Monkhorst and J. D. Pack, Phys. Rev. B **13**, 5188 (1976).

[47] D. D. Johnson, F. J. Pinski, and G. M. Stocks, Phys. Rev. B **30**, 5508 (1984).

[48] R. Zeller, J. Phys. Condens. Matter **16**, 6453 (2004).

[49] A. R. Denton and N. W. Ashcroft, Phys. Rev. A **43**, 3161 (1991).

[50] See Supplemental Material at http://link.aps.org/supplemental/10.1103/PhysRevLett.112.156401 for Fermi surface at $x < 0.6$, density of states, and lattice fits.

[51] Free energy change per atom is the formation energy plus the ideal mixing entropy, i.e., $\Delta s = (1/5)k_B T[x\log(x) + (1-x)\log(1-x)]$, with annealing $T = 1000$ K. The $1/5$ arises because Ba/K occupy only $1/5$ of all sites.

[52] T. Wolf (private communication).

[53] C. H. Lee, K. Kihou, H. Kawano-Furukawa, T. Saito, A. Iyo, H. Eisaki, H. Fukazawa, Y. Kohori, K. Suzuki, H. Usui, K. Kuroki, and K. Yamada, Phys. Rev. Lett. **106**, 067003 (2011).

[54] S. A. J. Kimber, A. Kreyssig, Y.-Z. Zhang, H. O. Jeschke, R. Valenti, F. Yokaichiya, E. Colombier, J. Yan, T. C. Hansen, T. Chatterji, R. J. McQueeney, P. C. Canfield, A. I. Goldman, and D. N. Argyriou, Nat. Mater. **8**, 471 (2009).